Room-Temperature Ferromagnetism of Flowerlike CuO Nanostructures

Daqiang Gao, Guijin Yang, Jinyun Li, Jing Zhang, Jinlin Zhang, and Desheng Xue*

Key Laboratory for Magnetism and Magnetic Materials of MOE, Lanzhou University, Lanzhou 730000, P. R. China

Received: June 29, 2010; Revised Manuscript Received: September 10, 2010

Flowerlike CuO nanostructures were prepared by the coprecipitation method with postannealing in air at different temperatures. The results of X-ray diffraction and Raman and X-ray photoelectron spectroscopies show that the samples annealed at 400, 600, and 800 °C have a typical monoclinic structure and are absent of impurity phases. Magnetic measurements indicate that all of the CuO nanostructures show room-temperature ferromagnetism, whereas CuO bulk presents paramagnetism. The saturation magnetization of the samples was found to increase with increasing annealing temperature. The fitting results of the O 1s XPS spectra for the three samples indicate that oxygen vacancies exist in the samples and that the variation of the oxygen vacancy concentration is in complete agreement with the variation of the saturation magnetization. When the samples were annealed in oxygen atmosphere, the ferromagnetism of the samples decreased enormously. These results confirm that the observed room-temperature ferromagnetism in flowerlike CuO nanostructures might originate from oxygen vacancies.

Introduction

Following the theoretical predictions of Dietl et al.,[1] many efforts have been devoted to search for magnetic semiconductors with Curie temperatures above room temperature in various host semiconductor materials (such as ZnO, TiO_2, In_2O_3, CuO, and SnO_2) by doping with 3d transition metals. The origin of room-temperature ferromagnetism (FM) in these materials has been attributed to the hybridization between the 3d state of the magnetic ions and the 2p state of oxygen.[2−7] However, the situation is challenged by the appearance of unexpected FM in pure HfO_2 thin films.[8] Recently, there have also been reports of room-temperature FM in pure metal oxides such as ZnO, MgO, CaO, Al_2O_3, CeO_2, and MoO_2 (films, powders, etc.), where the magnetism has been termed d^0-ferromagnetism to emphasize the fact that the observed room-temperature FM is not due to any partially filled d orbital but rather arises from moments induced by defects.[9−13] Moreover, the ferromagnetic-like behavior is induced in Au and ZnO nanoparticles by capping with some organic molecules.[14,15] First-principles calculations also reveal that the spin polarization on N and O atoms at the O-terminated ZnO(0001) surface might contribute to the FM in ZnO nanoparticles with capping oleylamine.[16] Although many reports have been published on the observation of room-temperature FM in these materials, the origin of the FM is still in debate and requires further investigation.

CuO, a p-type semiconductor with a narrow band gap (1.2 eV), exhibits great potential for broad applications in photoelectron chemical materials,[17] gas sensors,[18] lithium ion electrode materials,[19] field-emission emitters,[20,21] and heterogeneous catalysts.[22] Recently, Punnoose et al. prepared monoclinic CuO nanocrystals by the sol−gel method. They observed weak FM up to 330 K for small nanograins with grain sizes of $D < 10$ nm, whereas the magnetic ordering for the CuO grains with $D > 10$ nm was essentially similar to the antiferromagnetic ordering of bulk CuO.[23] Qin et al. also showed that CuO powders and thin films exhibit room-temperature FM, and they considered the observed FM to be related to oxygen vacancies.[24] More recently, based on both the experimental and theoretical works, it was suggested that the surface oxygen vacancies of nanostructures play an important role in inducing room-temperature FM.[25,26] Therefore, the surface morphology of a material seems to be able to modulate room-temperature FM as a result of different surface areas. Thus, it is valuable to investigate the relationship between the surface morphology and the FM of materials. In this work, different flowerlike CuO nanostructures were synthesized by a simple coprecipitation method with postannealing, and dependence of the magnetic properties on the morphology was investigated.

Experimental Section

CuO nanoparticles were prepared by the coprecipitation technique with the postannealing in air. Three grams of highly pure $Cu(NO_3)_2 \cdot 6H_2O$ was dissolved in a solution of 50 mL of deionized water, and NH_4OH solution was added drop by drop until a pH value of 10 was reached. The mixture was stirred for 4 h at room temperature and then dried at 50 °C for 6 h. When annealing the precursor, we first keep the temperature of the furnace at 400, 600, and 800 °C beforehand and then placed the precursor in the furnace. The annealing time for each sample was 3 h. Any possibility of magnetic contamination through accidental or trace impurities was meticulously avoided during sample preparation. A high-purity quartz boat without any metallic contamination was used for annealing of the samples in the furnace. The morphologies of the nanostructures were obtained by transmission electron microscopy (TEM, JEM-2010) and scanning electron microscopy (SEM, Hitachi S-4800). X-ray diffraction (XRD, X′ Pert PRO Philips instrument with Cu Kα radiation) was employed to study the structure of the samples. The vibration properties were characterized by Raman scattering spectral measurements, which were made on a Jobin-Yvon LabRam HR80 spectrometer (with the 532-nm line of a Torus 50 mW diode-pumped solid-state laser) under the backscattering geometry. The doping levels and the bonding characteristics were determined by X-ray photoelectron spectroscopy (XPS,

* Corresponding author. E-mail: xueds@lzu.edu.cn.

10.1021/jp106015t
Published on Web 10/08/2010

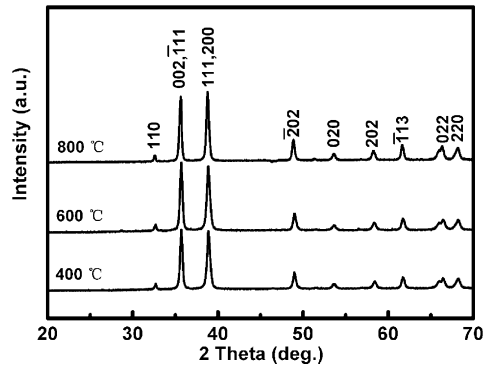

Figure 1. XRD patterns of CuO nanostructures annealed at 400, 600, and 800 °C.

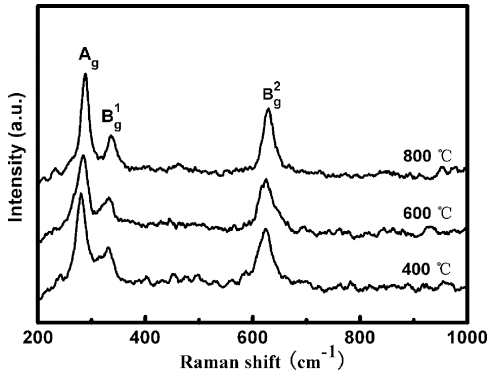

Figure 2. Raman spectra of CuO nanostructures annealed at 400, 600, and 800 °C.

VG ESCALAB 210). The measurements of magnetic properties were made using a Quantum Design MPMS magnetometer based on superconducting quantum interference device (SQUID) and a vibrating sample magnetometer (VSM, Lakeshore 7304).

Results and Discussion

Structural analysis of the CuO nanostructures was carried out by XRD, and the results are shown in Figure 1. All of the diffraction peaks can be indexed to a monoclinic phase of CuO (JCPDS 05-0661). No noticeable peaks introduced by impurities such as $Cu(OH)_2$ and Cu_2O can be detected. Additional information on the structure of the CuO nanostructures was obtained by Raman spectroscopy in the range of 200−1000 cm^{-1} measured at room temperature, and the results are shown in Figure 2. The CuO crystal belongs to the C_{2h}^6 space group with two molecules per primitive cell. One can find the zone-center Raman-active normal modes as $\Gamma_{RA} = 4A_u + 5B_u + A_g + 2B_g$,[27] which are three acoustic modes ($A_u + 2B_u$), six infrared-active modes ($3A_u + 3B_g$), and three Raman-active modes ($A_g + 2B_g$). In general, the modes at ca. 297, 346, and 631 cm^{-1} for all of the samples can be assigned to the A_g, B_g^1, and B_g^2 modes, respectively, which is consistent with the previous findings.[28] These results indicate that the CuO nanostructures that we prepared have a single phase and are highly crystalline in nature.

Parts a−c of Figure 3 show representative SEM images of the as-prepared CuO nanostructures, which were annealed at 400, 600, and 800 °C, respectively. The magnification of a single flowerlike aggregate from each nanostructure is shown in Figure 3A−C. From Figure 3a−c, it can be seen that the products are composed of a large amount of flowerlike aggregates and that most of them are uniform, with diameters ranging from 2 to 3 μm. For the magnified images, one can see that the aggregates

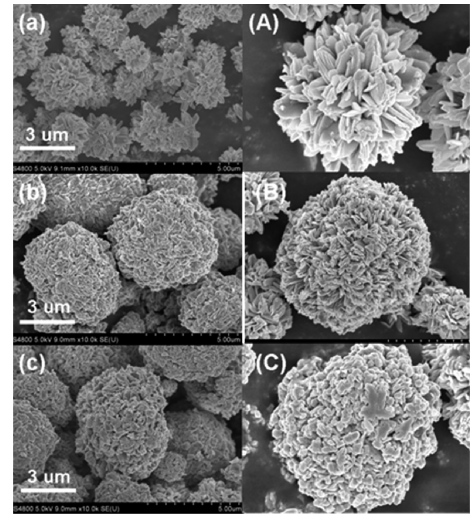

Figure 3. SEM images of the as-prepared CuO nanostructures annealed at (a) 400, (b) 600, and (c) 800 °C. The magnification of a single flowerlike aggregate for each sample is shown in A−C, respectively.

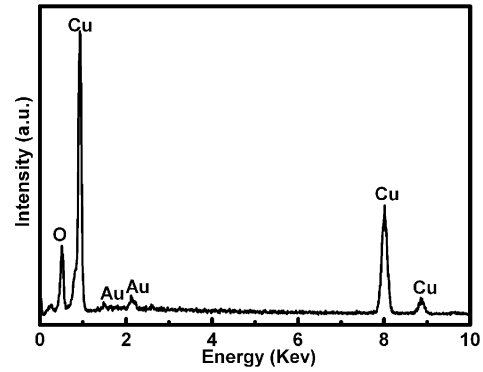

Figure 4. EDX spectrum of the CuO nanostructure annealed at 600 °C.

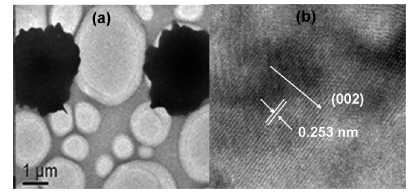

Figure 5. (a) TEM and (b) high-resolution TEM images of the CuO nanostructure annealed at 600 °C.

are mainly composed of numerous closely packed nanoplates extending from the inner part of the aggregates with lengths of about 320 and 230 nm for samples annealed at 400 and 600 °C, respectively. However, for the sample annealed at 800 °C, the flowerlike aggregates are composed of some nanoparticles with a size of 180 nm. The energy dispersive X-ray (EDX) spectra of thhe CuO nanostructure annealed at 600 °C in Figure 4 shows that only Cu and O are the elemental components, in addition to Au, which comes from the SEM testing process, implying no other impurity in fabricated samples. Figure 5 shows the morphology image of the sample annealed at 600 °C captured by TEM. From Figure 5a, it can be seen that the nanoplates congregate together and that the size of the flowerlike nanostructure is about 3 μm, which is consistent with the SEM results. Figure 5b shows the high-resolution TEM image of the corresponding CuO nanostructure. The lattice fringes between the two adjacent planes are 0.253 nm apart, which is equal to the lattice constant of the standard CuO (002) plane.[29]

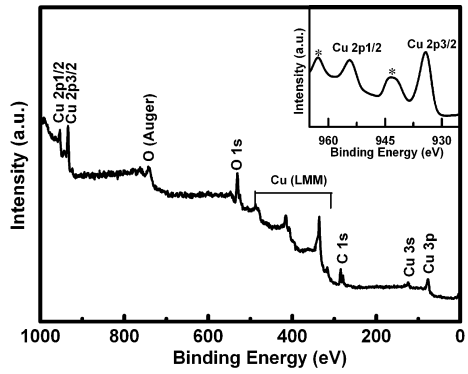

Figure 6

Figure 6. Representative XPS survey spectrum for the sample annealed at 600 °C. Inset: High-resolution scan of Cu 2p.

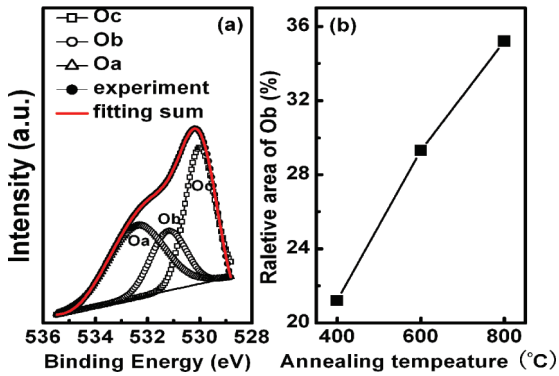

Figure 7. (a) Fitted XPS O 1s spectra of the sample annealed 600 °C. (b) Relative areas (percentages) of oxygen vacancies in samples annealed at different temperatures.

Further evidence for the purity and composition of the products was obtained by XPS, and the results show that the indexed peaks corresponded to C, O, and Cu for all of the CuO nanostructures annealed at different temperatures. A representative XPS spectrum of the CuO nanostructure annealed at 600 °C is shown in Figure 6. The inset shows the Cu 2p core-level XPS spectrum. For the Cu 2p spectrum, the peaks correspond to the core-level $2p_{3/2}$ and $2p_{1/2}$ transitions of copper at 933.6 and 953.6 eV, respectively. Meanwhile, satellites on the higher-binding-energy sides are also visible. These values are comparable to the values reported for Cu 2p levels in CuO.[28]

Figure 7a depicts the multicomponent fitting to the O 1s peak in sample annealing at 600 °C. The broad and asymmetric nature of the peak could be due to the various coordinations of oxygen in the nanostructure. As reported previously in the literature, the O 1s peak could be fitted with three peaks by Gaussian fitting.[30,31] The lowest-binding-energy peak located at 530.1 ± 0.2 eV (Oa) can be assigned to O^{2-} ion in CuO, surrounded by Cu atoms with their full complement of nearest-neighbor O^{2-} ions. The highest-binding-energy peak at 532.4 ± 0.2 eV (Oc) is usually attributed to the near-surface oxygen, oxygen atoms in carbonate ions, surface hydroxylation, adsorbed H_2O, or O_2. Interestingly, a new peak at 531.2 ± 0.2 eV (Ob) emerges. It has previously been reported that this peak could develop with increasing loss of oxygen and could be associated with O^{2-} ions in oxygen-deficient regions (O vacancies). Thus, the intensity of the medium-binding-energy component (Ob) might be related to the concentration of oxygen vacancies. It can be seen that the concentration of oxygen vacancies (Ob) increased with the annealing temperature (Figure 7b).

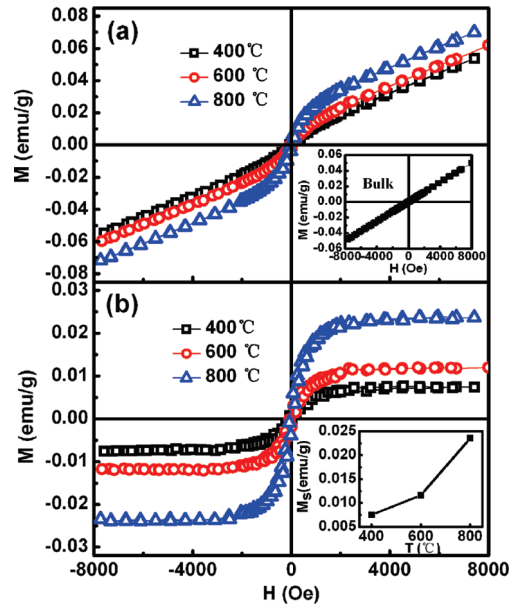

Figure 8. (a) $M-H$ curves for CuO nanostructures annealed at different temperatures, with the $M-H$ curve of bulk CuO shown in the inset. (b) $M-H$ curves for CuO nanostructures annealed at different temperatures after PM corrections, with the variation of the M_s dependence on the annealing temperature in the inset.

The contrasts in oxygen contents in the samples annealed at 400, 600, and 800 °C motivated us to carry out a comparative study on their magnetic properties. In examining the magnetic properties of these flowerlike CuO nanostructures, a careful consideration of whether contamination is responsible for the FM has to be made. All of the experimental procedures were carried out very carefully. The capsules used to hold the samples during the magnetic measurements were also checked carefully and showed no ferromagnetic signals. Extreme precautions were taken during different steps involved in the experimental process to avoid any magnetic contamination. Figure 8a shows the magnetization versus magnetic field ($M-H$) curves for the CuO nanostructures, which were investigated at room temperature by VSM under the maximum applied magnetic field of 8000 Oe. The hysteresis loops indicate that all of the CuO nanostructures had visible room-temperature FM, and the measured coercivities were 62, 87, and 67 Oe for the samples annealed at 400, 600, and 800 °C, respectively. Bulk CuO was obtained by annealing the precursor at 800 °C for 72 h, and its $M-H$ curve is shown in the inset of Figure 8a. It can be seen that bulk CuO shows paramagnetism (PM) at room temperature. The $M-H$ curves of the three samples after PM corrections are shown in Figure 8b, which indicate that the saturation magnetization (M_s) increased from 0.006 to 0.022 emu/g as the annealing temperature was increased from 400 to 800 °C.

From the original $M-H$ curves, it can be seen that strong PM signals exist in all of the samples excepting ferromagnetic phase. To confirm this, the temperature dependence of the magnetization ($M-T$) for the CuO nanostructure annealed at 600 °C was measured in the range of 2−300 K at 5000 Oe, and the results are shown in Figure 9. It can be seen that the curve shows a rapid decay of magnetization with increasing temperature in the low-temperature region, followed by a gradual decline in the magnetization that does not reach zero until 300 K, indicating a PM phase mixed with an FM phase for the sample. The absence of an FM transition in the $M-T$ plot indicates that the Curie temperature of this sample is over 300 K. The $M-T$ curve was fitted with a combination of the standard

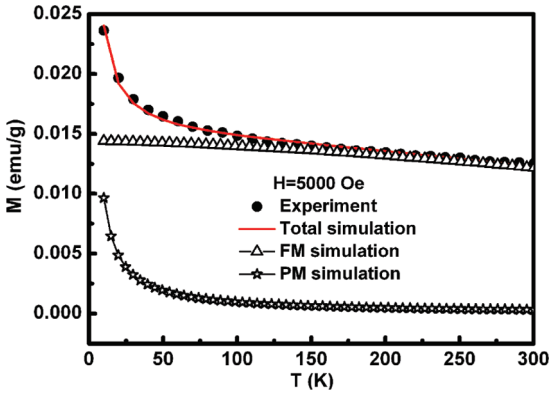

Figure 9. $M-T$ curve for the sample annealed 600 °C. The fitting result of the curve is shown by the solid line.

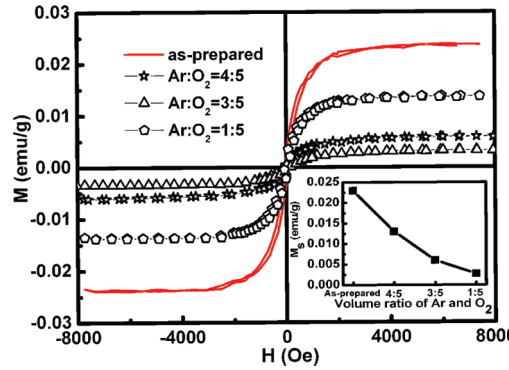

Figure 10. $M-H$ curves of the prepared sample (800 °C) about 1 h after annealing at different ratios of argon and oxygen.

3D spin-wave model for the FM phase and a curie law for the PM phase, as given by the equation

$$M(T) = M_{s0}(1 - AT^{3/2}) + CH/T \quad (1)$$

where C is the Curie constant, M_{s0} is the saturation magnetization at $T = 0$ K, and A is a coefficient correlated with the structure and properties of material. The best fit for the sample is shown by solid curve in Figure 7b, from which we obtained $M_{s0} = 0.01442$ emu/g and $C = 1.922 \times 10^{-5}$ emu·K/g·Oe. The good fit of the combination of the standard 3D spin-wave and the Curie model gives a mixed magnetic phase of the sample (FM and PM phases). From eq 1, the contributions of the FM and PM phases can be separated, as shown in Figure 9.

Because the possible presence of contamination has already been excluded, the FM for the CuO nanostructures must be an intrinsic property of materials. The surface spins are expected to dominate the measured magnetization because of their lower coordination and uncompensated exchange couplings.[32] The real reason for the FM of the CuO nanostructures here is supposed to have a relationship with only the unpaired electron spins resulting from the oxygen vacancies of the nanostructure. It is known that oxygen escape from a chemical bond because of heating can result in the unpaired electrons showing abnormal spin phenomena to introduce FM. In addition, the O 1s fitting results indicate that oxygen vacancies exist in the samples and the the variations of oxygen vacancies correspond to the variations of M_s. To further check the origin of FM in the CuO nanostructures, post-oxygen-annealing in different ratios of argon and oxygen was performed for the prepared sample (800 °C), where the total flow rate of gas was 100 SCCM (SCCM denotes standard cubic centimeters per minute). The resulting $M-H$ curves are shown in Figure 10, where the PM signal of the holder and the samples was subtracted from the measured magnetic signal. The data of the as-prepared sample (800 °C) are also included here for direct comparison. Usually, vacuum annealing effectively introduces some oxygen vacancies in oxides, whereas oxygen annealing reduces oxygen vacancies. It can be seen that M_s gradually decreased to 0.007 emu/g after 1 h of annealing as the oxygen ratio in the mixture of argon and oxygen was increased, indicating that oxygen vacancies play an important role in introducing FM into the flowerlike nanostructures. From the SEM results, it can be seen that the aggregates composed of flowerlike structures have different shapes and sizes, where the aggregate for the sample annealed at 800 °C has the largest surface area whereas the sample annealed at 400 °C has the smallest. At the same time, the O 1s fitting results for the three samples indicate that the concentration of oxygen vacancies increased as the annealing time increased. Therefore, it is suggested that the oxygen vacancies, especially the surface oxygen vacancies, dominate the observed FM in this case.

Conclusion

Flowerlike CuO nanostructures were synthesized by the simple coprecipitation method with postannealing. The morphology of the products revealed that the CuO nanostructures have different flowerlike shapes owing to the setting of the precursor at different annealing temperatures beforehand. The structural analysis indicated the products are the monoclinic phase, as further confirmed by the Raman results. Magnetic measurements indicated that all of the CuO nanostructures exhibited the room-temperature FM. The O 1s fitting results indicated that oxygen vacancies were present in the samples and that the variation of the oxygen vacancies corresponded to that of M_s for the three samples. Further, post-oxygen-annealing reduced the FM of the samples. This indicates that the FM in flowerlike CuO might originate from oxygen vacancies. Such flower-shaped CuO nanostructures could be involved in many possible applications in different fields.

Acknowledgment. This work was supported by the National Science Fund for Distinguished Young Scholars (Grant 50925103), the Keygrant Project of Chinese Minisity of Education (Grant 309027), the Fundamental Research Funds for the Central Universities (Grant Lzujbky-2009-162), and the National Nature Science Foundation of China (Grant 11034004).

References and Notes

(1) Dietl, T.; Ohno, H.; Matsukura, F.; Cibert, J.; Ferrand, D. *Science* **2000**, *287*, 1019.
(2) Gao, D. Q.; Zhang, J.; Yang, G. J.; Zhang, J. L.; Shi, Z. H.; Qi, J.; Zhang, Z. H.; Xue, D. S. *J. Phys. Chem. C* **2010**, *114*, 13477.
(3) Bryan, J. D.; Heald, S. M.; Chambers, S. A.; Gamelin, D. R. *J. Am. Chem. Soc.* **2004**, *126*, 11640.
(4) Chu, D. W.; Zeng, Y. P.; Jiang, D. L. *Appl. Phys. Lett.* **2008**, *92*, 182507.
(5) Li, Y. X.; Xu, M.; Pan, L. Q.; Zhang, Y. P.; Guo, Z. G.; Bi, C. *J. Appl. Phys.* **2010**, *107*, 113908.
(6) Wang, X. L.; Dai, Z. X.; Zeng, Z. *J. Phys.: Condens. Matter* **2008**, *20*, 045214.
(7) Kumar, E. S.; Venkatesh, S.; Ramachandra Rao, M. S. *Appl. Phys. Lett.* **2010**, *96*, 232504.
(8) Venkatesan, M.; Fitzgerald, C. B.; Coey, J. M. D. *Nature (London)* **2004**, *430*, 630.
(9) Xu, Q. Y.; Schmidt, H.; Zhou, S. Q.; Potzger, K.; Helm, M.; Hochmuth, H.; Lorenz, M.; Setzer, A.; Esquinazi, P.; Meinecke, C.; Grundmann, M. *Appl. Phys. Lett.* **2008**, *92*, 082508.

(10) Gao, D. Q.; Li, J. Y.; Li, Z. X.; Zhang, Z. H.; Zhang, J.; Shi, H. G.; Xue, D. S. *J. Phys. Chem. C* **2010**, *114*, 11703.
(11) Kapilashrami, M.; Xu, J.; Rao, K. V.; Belova, L.; Carlegrim, E.; Fahlman, M. *J. Phys.: Condens. Matter* **2010**, *22*, 345004.
(12) Ge, M. Y.; Wang, H.; Liu, E. Z.; Liu, J. F.; Jiang, J. Z.; Li, Y. K.; Xu, Z. A.; Li, H. Y. *Appl. Phys. Lett.* **2008**, *93*, 062505.
(13) Thakur, P.; Cezar, J. C.; Brookes, N. B.; Choudhary, R. J.; Prakash, R.; Phase, D. M.; Chae, K. H.; Kumar, R. *Appl. Phys. Lett.* **2009**, *94*, 062501.
(14) Crespo, P.; Garcia, M. A.; Fernandez-Pinel, E.; de la Venta, J.; Merino, J. M.; Quesada, A.; Hernando, A. *Acta Phys. Pol. A* **2008**, *113*, 515.
(15) Garcia, M. A.; Merino, J. M.; Fernández Pinel, E.; Quesada, A.; de la Venta, J.; Ruíz González, M. L.; Castro, G. R.; Crespo, P.; Llopis, J.; González-Calbet, J. M.; Hernando, A. *Nano Lett.* **2007**, *7*, 1489.
(16) Liu, J. F.; Liu, E. Z.; Wang, H.; Su, N. H.; Qi, J.; Jiang, J. Z. *Nanotechnology* **2009**, *20*, 165702.
(17) Chaudhary, Y. S.; Agrawal, A.; Shrivastav, R.; Satsangi, V. R.; Dass, D. *Int. J. Hydrogen Energy* **2004**, *29*, 131.
(18) Chowdhuri, A.; Gupta, V.; Sreenivas, K.; Kumar, R.; Mozumdar, S.; Patanjali, P. K. *Appl. Phys. Lett.* **2004**, *84*, 1180.
(19) Gao, X. P.; Bao, J. L.; Pan, G. L.; Zhu, H. Y.; Huang, P. X.; Wu, F.; et al. *J. Phys. Chem. B* **2004**, *108*, 5547.
(20) Hsieh, C. T.; Chen, J. M.; Lin, H. H.; Shih, H. C. *Appl. Phys. Lett.* **2003**, *83*, 3383.
(21) Chen, J.; Deng, S.; Xu, N.; Zhang, W.; Wen, X.; Yang, S. *Appl. Phys. Lett.* **2003**, *83*, 746.
(22) Switzer, J. A.; Kothari, H. M.; Poizot, P.; Nakanishi, S.; Bohannan, E. W. *Nature* **2003**, *425*, 490.
(23) Punnoose, A.; Magnone, H.; Seehra, M. S.; Bonevich, J. *Phys. Rev. B* **2001**, *64*, 174420.
(24) Qin, H. W.; Zhang, Z. L.; Liu, X.; Zhang, Y. J.; Hu, J. F. *J. Magn. Magn. Mater.* **2010**, *322*, 1994.
(25) Zhang, L.; Ge, S. H.; Zuo, Y. L.; Zhang, B. M.; Xi, L. *J. Phys. Chem. C* **2010**, *114*, 7541.
(26) Wang, C.; Ge, M. Y.; Jiang, J. Z. *Appl. Phys. Lett.* **2010**, *97*, 042510.
(27) Xu, J. F.; Ji, W.; Shen, Z. X.; Li, W. S.; Tang, S. H.; Ye, X. R.; Jia, D. Z.; Xin, X. Q. *J. Raman Spectrosc.* **1999**, *30*, 413.
(28) Wang, X.; Xi, G.; Xiong, S.; Liu, Y.; Xi, B.; Yu, W.; Qian, Y. *Cryst. Growth Des.* **2007**, *7*, 930.
(29) Teng, F.; Yao, W. Q.; Zheng, Y. F.; Ma, Y. T.; Teng, Y.; Xu, T. G.; Liang, S. H.; Zhu, Y. F. *Sens. Actuators B* **2008**, *134*, 761.
(30) Pandey, B.; Ghosh, S.; Srivastava, P.; Kumar, P.; Kanjilal, D.; Zhou, S.; Schmidt, H. *J. Appl. Phys.* **2010**, *107*, 023901.
(31) Chen, M.; Wang, X.; Yu, Y. H.; Pei, Z. L.; Bai, X. D.; Sun, C.; Huang, R. F.; Wen, L. S. *Appl. Surf. Sci.* **2000**, *158*, 134.
(32) Dutta, D. P.; Sharma, G.; Manna, P. K.; Tyagi, A. K.; Yusuf, S. M. *Nanotechnology* **2008**, *19*, 245609.

JP106015T